01 Jan 2023

Improved Quantification Of Defect Cross-Section For Active Microwave Thermography

Logan M. Wilcox

Kristen M. Donnell
Missouri University of Science and Technology, kmdgfd@mst.edu

Improved Quantification of Defect Cross-Section for Active Microwave Thermography

Logan M. Wilcox and Kristen M. Donnell
Microwave Sensing (μSense) Laboratory
Department of Electrical and Computer Engineering
Missouri University of Science and Technology
Rolla, Missouri, USA
{lmwc65;kmdgfd}@mst.edu

2023 IEEE International Instrumentation and Measurement Technology Conference (I2MTC) | 978-1-6654-5383-7/23/$31.00 ©2023 IEEE | DOI: 10.1109/I2MTC53148.2023.10176038

Abstract—Active microwave thermography (AMT) is an integrated nondestructive testing and evaluation (NDT&E) technique that features a microwave-based excitation and subsequent thermographic inspection via an infrared camera. AMT has been successfully employed in several industries including aerospace and civil for NDT&E inspections. Since the excitation is microwave-based, an antenna is used to irradiate the sample under test and hence the heating pattern will vary spatially (following the antenna pattern). This nonuniform thermal excitation may limit the ability of AMT to quantify defect cross-sections. Therefore, this work seeks to expand the capabilities of AMT by incorporating a post-processing technique to improve defect cross-section quantification. Specifically, an approach based on the temperature gradient is considered, with results compared to other well-established approaches. The effect of noise is also considered. The results, from both simulation and measurement, indicate that the temperature gradient approach provides the least amount of error in defect cross-section quantification.

Keywords—Active Microwave Thermography (AMT), Canny Edge Detection, Defect Cross-Section Quantification, Nondestructive Testing and Evaluation (NDT&E), Nonuniform Heating, Temperature Gradient

I. Introduction

The field of nondestructive testing and evaluation (NDT&E) includes a multitude of techniques used to inspect, detect, and quantify defects within a specimen under test (SUT). To effectively select a technique for a given inspection need, several factors must be considered including material properties, type of defect, defect and structure orientation, defect location, and so forth. Thermography is one such NDT&E technique that has found continued success in the areas of civil infrastructure, aerospace, and space, amongst others. Thermography is an attractive technique due to its large-scale inspection potential, established signal processing, and relatively easy-to-interpret results [1]. In recent years, thermography has expanded from the traditional flash lamp excitation to include other types of thermal excitation including laser [2], induction [3], ultrasound transducer [4], and microwave [5]-[8]. When incorporating a microwave excitation, the approach is commonly referred to as Active Microwave Thermography, or AMT. AMT utilizes high frequency electromagnetic energy to induce a thermal response in the SUT. This thermal response is usually achieved through dielectric absorption (i.e., heating) within the SUT and takes place volumetrically (as opposed to solely on the surface such as the case of traditional flash lamp thermography). To this end, the presence of a defect effects the heat diffusion and is subsequently measured (on the surface of the SUT) by an infrared camera. Although a recently developed technique, AMT has found success in a variety of infrastructure- and aerospace-related inspections including detection of water ingress, delaminations, voids, and flat-bottom holes [5]-[8]. Additionally, AMT is advantageous over traditional thermography since the electromagnetic excitation source allows for selective and localized heating, reduced temperature increase during inspection, and designability for a specific SUT (i.e., frequency and polarization).

AMT utilizes an antenna to radiate the electromagnetic energy towards the SUT. Generally speaking, antennas have unique radiation patterns (i.e., transmitted electric and magnetic fields) which are spatially nonuniform. These nonuniform electric and magnetic fields, incident on the SUT, cause a related nonuniform thermal excitation. This nonuniformity in the thermal excitation brings about the potential for defects to be masked (i.e., a false negative inspection result) or a nonphysical defect to be detected (e.g., a false positive inspection result). Additionally, when a defect is detected, the nonuniform thermal excitation causes uncertainty in the quantification of the cross-section of a defect, making defect quantification challenging and/or error prone. To this end, this research expands on AMT by proposing an image processing method, based on the gradient of temperature distribution, that facilitates improved quantification of defect cross-sections.

II. Background

As previously mentioned, in AMT, the thermal excitation is usually achieved through dielectric absorption of the incident electromagnetic energy (as opposed to conduction heating). In general, dielectric materials are described electromagnetically by their complex dielectric properties. When referenced to free space, the relative dielectric properties are denoted as $\varepsilon_r = \varepsilon_r' - j\varepsilon_r''$, where the real part ($\varepsilon_r'$) is referred to as the permittivity and represents the ability of a material to store electric energy. The imaginary part (ε_r'') is referred to as the loss factor and represents the ability of a material to absorb electric energy. The loss factor is of particular interest in AMT, as it is

the loss factor that facilitates heat generation from incident electromagnetic energy. This generated heat, Q, is defined as:

$$Q = 2\pi f \varepsilon_0 \varepsilon_r'' |E|^2 \quad (1)$$

where f is the frequency, ε_0 is the permittivity of free space, and $|E|$ is the magnitude of the incident electric field. This induced heat source (Q) causes a resulting surface (spatial) temperature distribution, T, which is defined as the temperature increase of the SUT due to the presence of the defect. The relationship between Q and T is described as [9]:

$$\left(\frac{\partial}{\partial t} - \alpha \nabla^2\right) T = \frac{1}{\rho c} Q \quad (2)$$

where α, ρ, and c denote thermal diffusivity, density, and specific heat, respectively, of the material through which the heat diffuses. From Eq. (2), an expression for the surface temperature distribution, T, after t seconds of microwave illumination can be derived to describe the total amount of absorbed electromagnetic energy without considering losses (i.e., a 1st order approximation), and is defined as the following:

$$T(t) = \frac{1}{\rho c} Q\, t \quad (3)$$

As mentioned above, the thermal response varies spatially and temporally due to the spatially-varying electromagnetic excitation and presence of the defect. To this end, one way to quantify the thermal spatial variation is through the application of a gradient. The concept of gradient can be described as the rate of change in a specified direction (i.e., a directional derivative). With the goal of quantifying a defect cross-section in mind, the gradient is applied to the surface temperature (on the plane of the inspection surface) in two orthogonal directions. When the gradient is equal to zero, it is indicative of a local maximum or minimum. To this end, the gradient is utilized in this work to determine the maximum temperature fluctuation between the defect and the structure (i.e., the largest temperature disparity on the surface of the SUT) and is applied to Eq. (3) as:

$$\nabla_{xy} T(t) = \nabla_{xy} \frac{1}{\rho c} Q\, t \quad (4)$$

where ∇_{xy} is the gradient operator as applied in two orthogonal directions (i.e., horizontally, x, and vertically, y). It is this quantity, $T(t)$, that is measured, analyzed through the gradient, and reported.

III. SIMULATIONS

To illustrate the capabilities of this gradient-based cross-section quantification approach, coupled full wave electromagnetic-thermal simulations were completed using CST MultiPhysics Studio™. The SUT was assumed to be a rubber structure undergoing water ingress, as is illustrated in Fig. 1. The cross-section of the SUT is 10 cm × 10 cm, with a thickness of 1.3 cm. The assumed water ingress has a cross-section of 4 cm × 4 cm and a thickness of 0.0375 cm (equivalent to a volume of 0.05 mL) and is located 0.1 cm from the inspection surface. The relevant electromagnetic and thermal properties for the water and rubber are shown in Table 1. As seen, the water ingress (defect within the SUT) has a high electric loss factor [10], while the rubber is assumed to be a low loss material [11]. Therefore, it will not undergo heating in the same capacity as the defect (i.e., the loss factor of the water is magnitudes larger than that of the rubber).

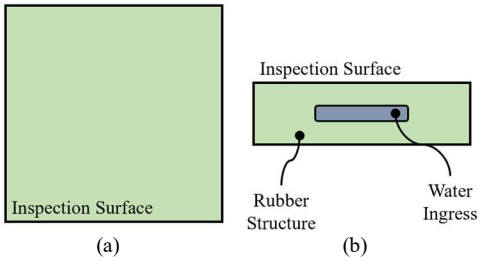

Fig. 1. Top (a) and side (b) illustrative views of the SUT.

During an AMT inspection, the water absorbs the electric field radiated from the antenna and becomes a volumetric heat source. The heat generated from the water then diffuses through the surrounding rubber structure, eventually reaching the inspection surface and hence can be observed. For this simulation, 50 W of electromagnetic energy is radiated from a standard gain horn antenna (aperture dimensions of 23 cm × 17 cm), placed 13 cm from the surface (i.e., the lift-off) of the SUT. A frequency of 2.4 GHz was used because water has a particularly high absorption of electromagnetic energy at this frequency [5], [10]. The simulation assumed a heating time of 300 seconds, and the thermal boundaries of the SUT are considered adiabatic.

Table 1: Electromagnetic and thermal properties of water and rubber [10]-[13]

Material	***Property***	***Value***
Water	Relative Permittivity, ε_r'	77
	Relative Loss Factor, ε_r''	9
Rubber	Relative Permittivity, ε_r'	2.4
	Relative Loss Factor, ε_r''	0
	Thermal Diffusivity, α	0.086 mm²/s
	Thermal Conductivity, k	0.16 W/m²·K
	Specifc Heat, c	2000 J/kg·K
	Density, ρ	930 kg/m³

Fig. 2 displays the normalized thermal surface profile of the SUT at t = 300 sec. The dashed white line in this image indicates the location of the cross-section of the water ingress within the rubber structure. As seen, while the presence of the defect is obvious, this image gives no clear indication of the specific cross-section of the defect. Moreover, without *a-priori* knowledge of the shape of the ingress (a square), these results may be interpreted to indicate a circular area of water. In reality, the circular heating pattern is a result of the spatial variation of the incident electromagnetic energy. Hence, post-processing

that can reduce the impact of the non-uniform thermal generation is of interest. To this end, post-processing techniques are considered to improve the ability of AMT to quantify the cross-section of the defect.

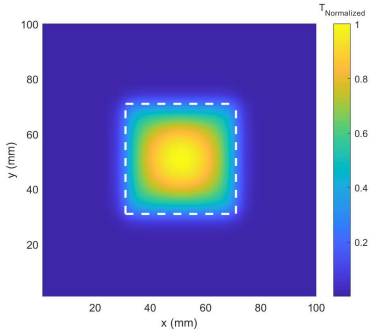

Fig. 2. Simulated unprocessed thermal surface profile.

To begin, existing signal/image processing routines built into MATLAB™, a commonly used signal processing software, are considered. As such, the built-in *Contour* function was considered as a cost-effective and simple solution to the AMT defect cross-section quantification problem. The *Contour* function was implemented on the data of Fig. 2 using 1, 5, 10, 25, and 50 contour regions, with the results shown in Fig. 3. As seen, each of the results provide a (potential) visual estimation of the defect's cross-section. Taking the result of Fig. 3a, for example, a cross-section estimation is 3.5 cm × 3.5 cm. In this case, the error can be calculated as:

$$\%\ ERROR = \frac{Calculated - Actual}{Actual} \times 100 \qquad (6)$$

where *Calculated* is the estimated result and *Actual* is the true (*a-priori* known) cross-section. Additionally, when the error is positive, this indicates that the cross-section was overestimated, while a negative error indicates an underestimation. In this case (Fig. 3a), the error is -12.5% for both orthogonal directions. For Fig. 3b and Fig. 3c, the error may be reduced, depending on what contour is selected for analysis. This, in fact, illustrates the problem with this approach for cross-section estimation; it requires interpretation and hence will have varying degrees of accuracy. In addition, when the contour regions are increased to 25 and beyond, (i.e., Fig. 3d and Fig. 3e), the image becomes exceedingly more difficult to interpret as it relates to the true cross-section. As a result, the MATLAB™ *Contour* function is not considered a reliable method for improving quantification of the defect cross-section.

Another image processing function included in MATLAB™ is *Edge*. *Edge* is comprised of a multitude of different edge detection techniques including Sobel [14], LoG [14], and Canny [14], [15]. For this work, the Canny technique within MATLAB™ *Edge* was selected because, when compared to other edge detection techniques, it performs best in noisy environments [14]. Canny utilizes a Gaussian filter to remove noise, then computes the gradient for each pixel within a given image. A non-maximum suppression is applied followed by a doubling threshold such that any gradient value below 0.3 is set to zero. Finally, a hysteresis is applied to the image, and it is normalized to the maximum value [16]. This technique was applied to the simulated results of Fig. 2, with the results provided in Fig. 4. As seen, the application of Canny significantly improves the image, with the calculated cross-section of 3.8 cm × 3.8 cm and an error of -5% in both directions.

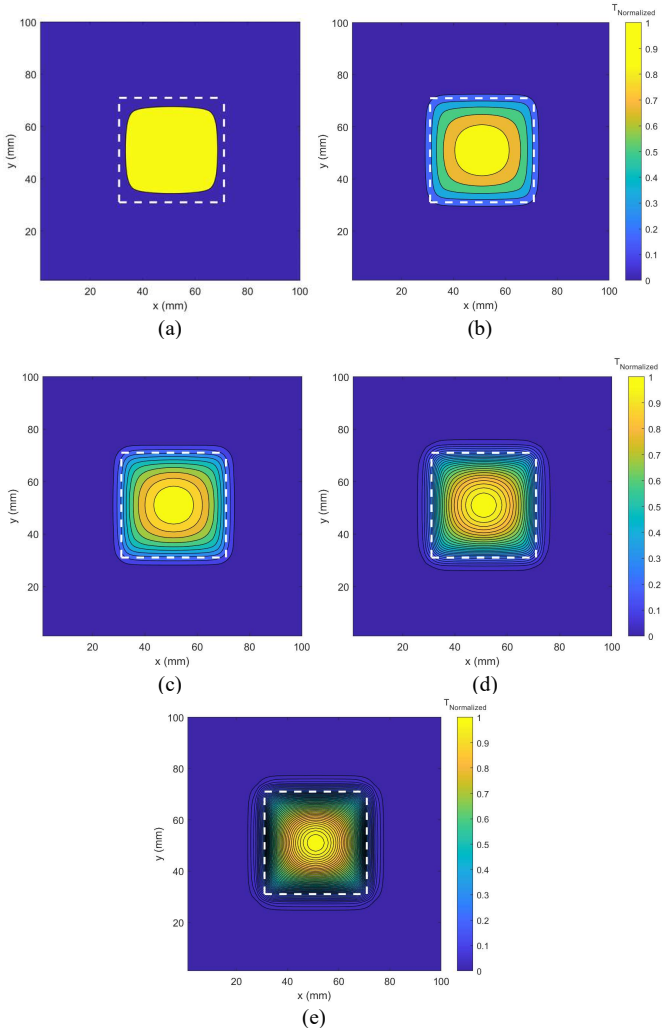

Fig. 3. MATLAB™ *Contour* function implemented on the thermal surface profile of Fig. 2 with 1 (a), 5 (b), 10 (c), 25 (d), and 50 (e) contour regions.

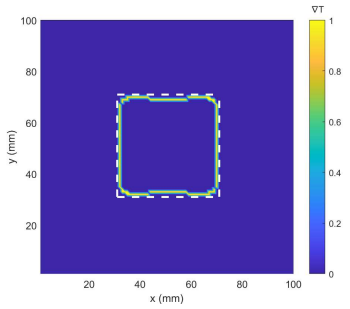

Fig. 4. Canny-processed thermal surface profile.

While the total error from Canny is better than that of the *Contour* approach, further improvement is desirable. To this end, the gradient method outlined above and shown in Eq. (4) is applied to the results of Fig. 2, with the results shown in Fig. 5a.

As seen, the results from this method compare well to the white-dashed line (indicating the true cross-section of the defect), with an error of -2.5% in both directions. This is an improvement over the Canny approach by a factor of 2. Lastly, to facilitate easy comparison of the error in all four cases, the error is summarized in Table 2, with the improvements mentioned above being evident.

Table 2: Cross-Section Estimation and Error for Fig. 2-Fig. 5a

Case	*Cross-Section (cm × cm)*	*X-Error (%)*	*Y-Error (%)*
Raw	2.1 × 2.1	-47.5	-47.5
Contour	3.5 × 3.5	-12.5	-12.5
Canny	3.8 × 3.8	-5	-5
Gradient	3.9 × 3.9	-2.5	-2.5

A final aspect that must be considered is the effect of noise when utilizing the gradient function for post-processing. To this end, 30 dBW of random white Gaussian noise was added to the unprocessed simulation results of Fig. 2, with the resultant image shown in Fig. 5b. With the addition of noise, the estimated defect cross-section is 3.9 cm × 4 cm (i.e., -2.5% error in the horizontal and 0% error in the vertical orthogonal directions). It is interesting to note that here, the error reduces with the inclusion of noise. In other words, the unprocessed simulation results provide an underestimation of the defect cross-section, and the addition of noise reduces this underestimation. This is due to the fact that the noise reduces the thermal disparity between the surrounding structure (rubber) and defect (water ingress). Hence, the error in estimated cross-section is reduced. To better illustrate this phenomenon, the spatial temperature variation in the horizontal direction (at the vertical point of 50 mm of the defect shown by the black dashed line in Fig. 5a and Fig. 5b) is shown in Fig. 6.

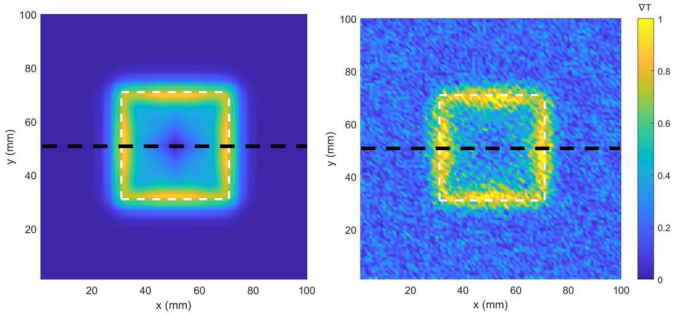

(a) (b)

Fig. 5. $\nabla_{xy}T$ of Fig. 2 without (a) and with (b) noise.

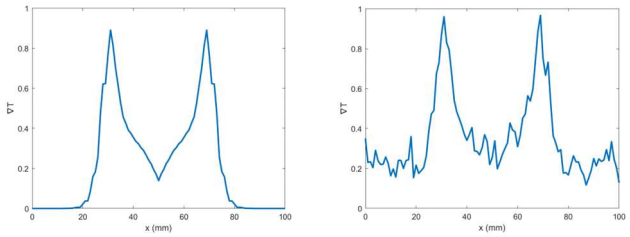

(a) (b)

Fig. 6. Simulated temperature spatial distribution across the middle of the defect without (a) and with (b) noise.

As seen in Fig. 6a (without noise), there is a gradient range of ~0.09 °K from rubber to water ingress. In addition, the temperature gradient between the rubber and defect center differs by ~0.02 °K. However, as shown in Fig. 6b (with noise), there is a gradient range of ~0.07 °K and the rubber region (0 – 20 mm and 80 – 100 mm) has approximately the same temperature gradient as that of the center of the defect. Therefore, the local minimum of the temperature gradient in the defect is nominally equivalent to that of the local minimum of the temperature gradient of the surround structure (i.e., Fig. 6b). This behavior is clearly a result of the noise level considered, but for the noise level considered here (30 dBW), the ability to quantify the cross-section of a defect is improved.

IV. Measurements

To further illustrate the improvement offered by the gradient-based cross-section quantification approach, AMT measurements were conducted on a SUT consisting of a rubber structure with a cross-section of 16 cm × 16 cm and thickness of 1.3 cm. The SUT contained a 4 cm × 4 cm paper towel (represented by the dashed, white line in the following images) placed 0.1 cm from the inspection surface that held 1 mL of water. A paper towel was used to hold the water because encompasses a low volume and has low permittivity and loss factor, making in minimally intrusive on the overall experimental results. The SUT was placed on polystyrene foam to avoid any thermal loss on the back side of the SUT (i.e., an adiabatic condition). An illustration of the AMT system used for these measurements can be seen in Fig. 7. The system consists of a computer, standard gain horn antenna (aperture dimensions of 23 cm × 17 cm), 50-watt power amplifier, FLIR T430sc infrared camera (thermal sensitivity of 30 m°K), data acquisition unit (DAQ), and microwave source (operating at 2.4 GHz). The heating time was 300 seconds.

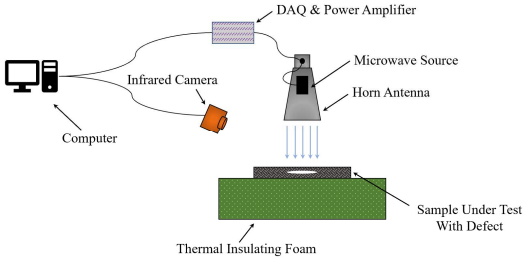

Fig. 7. Schematic of the AMT system.

Primary uncertainties that may affect measurement results include changes in ambient temperature, air flow over the SUT, and fluctuations in the water ingress cross-section. To

control/reduce the impact of fluctuations in ambient temperature, the temperature of the SUT prior to microwave excitation was measured and subsequently removed from AMT results prior to processing. Additionally, all AMT measurements are performed in a controlled, indoor environment to minimize changes in ambient temperature and air flow during the measurement process. Regarding the potential for water displacement, after each measurement, the location on the rubber samples where the wet paper towel (i.e., water) was placed flush contained small (visually evident) amounts of water. This area was measured (on both pieces of rubber) to ensure that the water remained within the intended cross-section. For all measurement sets, the cross-section remained as intended (i.e., 4 cm × 4 cm).

Fig. 8 displays the normalized (to the maximum and relative to ambient) surface thermal profiles for the following cases: unprocessed/raw data (a), processed using a 10-region contour (b), processed using the Canny algorithm (c), and processed using the gradient-based approach of Eq. 4 (d). Cross-section estimations for each case (with error) can be found in Table 3.

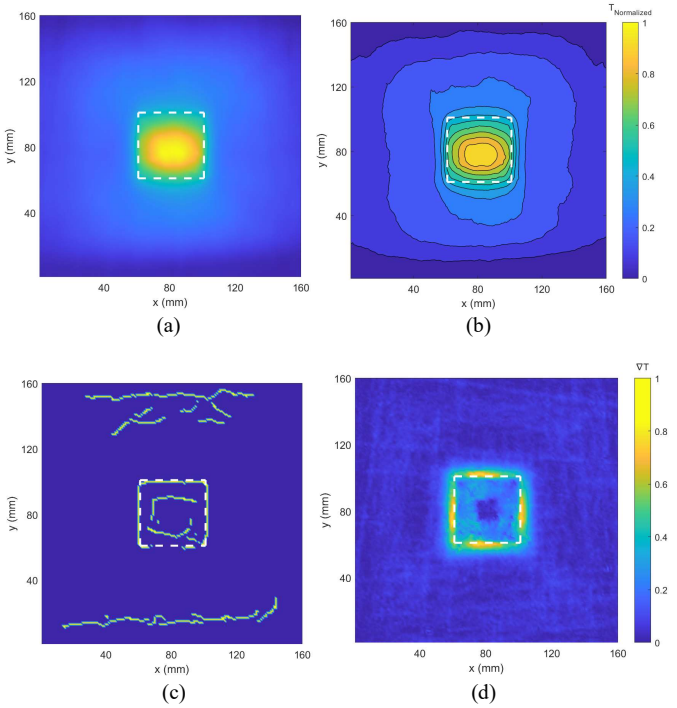

Fig. 8. Unprocessed (a), 10-region contour (b), Canny (c), and gradient-based (d) images for measurement results for 1 mL water.

As was the case for the simulated results above, the unprocessed and contour-processed images do not provide a clear indication of the defect cross-section. Canny processing (Fig. 8c) does provide a clear estimation of the cross-section, however this approach also includes additional indications within the known defect area. When comparing these false edges to the unprocessed image (i.e., Fig. 8a), these false edges align with the temperature increase within the water resulting from the antenna pattern directly. Therefore, in such cases, Canny is unreliable as it is susceptible to the heating pattern that results from the spatial distribution of the incident electromagnetic energy. Lastly, Fig. 8d displays the gradient-based approach. Here, the cross-section of the water ingress within the SUT can be seen clearly by the location of the maximum temperature gradient, with the influence of the heating pattern substantially reduced as compared to that of Canny (Fig. 8c). In addition, this approach provides the most accurate estimation of the defect cross-section, 4.1 cm × 4 cm, with the least amount of error (see Table 3).

A last set of measurements were completed using the same SUT but with a reduced water volume of 0.5 mL. Fig. 9 displays the surface thermal profile of this measurement and processed using the same approaches as Fig. 8. Cross-section estimation and error for each case can be found in Table 4. Here, the most accurate cross-section estimation is 4.2 cm × 4.1 cm as determined by the gradient-based approach. In other words, even with a reduction in volume of water and hence a reduced temperature increase (2.82 °K as opposed to 3.30 °K) on the inspection surface, the gradient-based post-processing approach still results in the most accurate outcome.

Table 3: Cross-section estimation and error for results of Fig. 8

Case	*Cross-Section (cm × cm)*	*X-Error (%)*	*Y-Error (%)*
Raw	3.1 × 2.3	-22.5	-42.5
Contour	4.2 × 3.6	+5	-10
Canny	4.2 × 4.1	+5	+2.5
Gradient	4.1 × 4.0	+2.5	+0

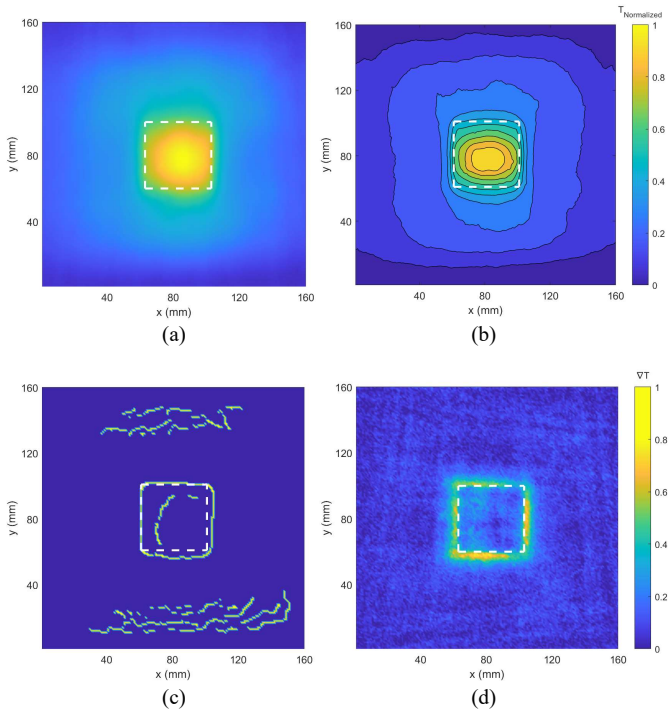

Fig. 9. Unprocessed (a), 10-region contour (b), Canny (c), and gradient-based (d) images for measurement results for 0.5 mL water.

Table 4: Cross-Section Estimation and Error for Fig. 9

Case	*Cross-Section (cm × cm)*	*X-Error (%)*	*Y-Error (%)*
Raw	3.0 × 2.9	-25	-27.5
Contour	4.5 × 5.3	+12.5	-32.5
Canny	4.4 × 4.7	+10	+17.5
Gradient	4.2 × 4.1	+5	+2.5

It is worth noting that there is a slight spatial bias (which translates to error) in most measurement results (raw and processed in Fig. 8 and Fig. 9, with the corresponding error shown in Tables 3 and 4, respectively) in the y-direction. This bias is attributed to the effect of the inherent antenna pattern of the radiating antenna.

V. Conclusion

Active Microwave Thermography, or AMT, is a relatively new thermographic inspection approach that features a high frequency-based thermal excitation. This thermal excitation is achieved by irradiating a sample under test with electromagnetic energy via an antenna. Since an antenna is used, the incident energy and hence the thermal excitation is dependent upon the antenna pattern (i.e., spatial variation of the incident energy). As such, this variation can cause errors in defect cross-section quantification. To this end, this work considers several well-known post-processing approaches along with a new approach based on temperature gradient. Simulated and measurement results indicate that the gradient-based approach performs better (with less error) than the other approaches considered.

Acknowledgment

This work was partially supported by the Kummer Innovation and Entrepreneurship Doctoral Fellowship.

References

[1] X. P. Maldague, “Theory and Practice of Infrared Technology for Nondestructive Testing”. New York, NY, USA: Wiley, 2001.

[2] Y. An J. M. Kim and H. Sohn "Laser lock-in thermography for detection of surface-breaking fatigue cracks on uncoated steel structures" NDT E Int. vol. 65 pp. 54-63 Jul. 2014.

[3] M. Noethen K.-J. Wolter and N. Meyendorf "Surface crack detection in ferritic and austenitic steel components using inductive heated thermography" Proc. 33rd IEEE Int. Spring Seminar Electron. Technol. (ISSE) pp. 249-254 May 2010.

[4] Mendioroz, A., R. Celorrio, and A. Salazar. "Ultrasound excited thermography: an efficient tool for the characterization of vertical cracks." Measurement Science and Technology, vol. 28, no. 11, Oct. 2017.

[5] A Mirala, A. Foudazi, M. T. Ghasr, and K. M. Donnell, “Active Microwave Thermography to Detect and Locate Water Ingress,” IEEE Trans. Instrum. Meas., vol. 69, no. 12, pp. 9774-9783, Dec. 2020.

[6] A. Foudazi, C. A. Edwards, M. T. Ghasr, and K. M. Donnell, “Active Microwave Thermography for Defect Detection of CFRP-Strengthened Cement-Based Materials,” IEEE Trans. Instrum. Meas., vol. 65, no. 11, pp. 2612-2620, Nov. 2016.

[7] A. Mirala, M. T. A. Qaseer and K. M. Donnell, "Health Monitoring of RAM-Coated Structures by Active Microwave Thermography," in IEEE Transactions on Instrumentation and Measurement, vol. 70, pp. 1-11, 2021.

[8] A. Mirala and K. M. Donnell. “Active Microwave Thermographic Measurement of In-Plane Thermal Diffusivity,” in Proc. IEEE Int. Instrum. Meas. Technol. Conf. (I2MTC), May 2020, pp. 1-5.

[9] J. H. Lienhard IV, and J. H. Lienhard V, A Heat Transfer Textbook, 4th ed., Cambridge, Massachusetts, USA: Philogiston, 2017.

[10] U. Kaatze, “Complex permittivity of water as a function of frequency and temperature,” J. Chem. Eng. Data, vol. 34, no. 4, pp. 371–374, Oct. 1989.

[11] M. Ghasr, D. Simms, and R. Zoughi, “Multimodal solution for a waveguide radiating into multilayered structures-dielectric property and thickness evaluation,” IEEE Trans. Instrum. Meas., vol. 58, no. 5, pp. 1505–1513, May 2009.

[12] W. M. Haynes, Ed., CRC Handbook of Chemistry and Physics. Boca Raton, FL, USA: CRC Press, 2016.

[13] E. M. Ortt et al, “A Device for Evaluating the Multiaxial Finite Strain Thermomechanical Behavior of Elastomers and Soft Tissues,” Journal of Applied Mechanics, vol. 67, pp. 465-471, Sep. 2000.

[14] R. Maini, H. Aggarwal, "Study and Comparison of Various Image Edge Detection Techniques," in International Journal of Image Processing (IJIP), vol. 3, no. 1, pp. 1-11, Feb. 2009.

[15] J. Canny, "A Computational Approach to Edge Detection," in IEEE Transactions on Pattern Analysis and Machine Intelligence, vol. PAMI-8, no. 6, pp. 679-698, Nov. 1986.